Comparison of atomic force microscopy force curve and solvation structure studied by integral equation theory

Hashimoto, Kota
Amano, Ken-ichi
Nishi, Naoya
Onishi, Hiroshi
Sakka, Tetsuo

(Citation)
Journal of Chemical Physics,154(16):164702

(Issue Date)
2021-04-28

(Resource Type)
journal article

(Version)
Version of Record

The Journal of Chemical Physics ARTICLE scitation.org/journal/jcp

Comparison of atomic force microscopy force curve and solvation structure studied by integral equation theory

Cite as: J. Chem. Phys. 154, 164702 (2021); doi: 10.1063/5.0046600
Submitted: 4 February 2021 • Accepted: 6 April 2021 •
Published Online: 22 April 2021

Kota Hashimoto,[1,a)] Ken-ichi Amano,[2] Naoya Nishi,[1] Hiroshi Onishi,[3] and Tetsuo Sakka[1]

AFFILIATIONS

[1] Department of Energy and Hydrocarbon Chemistry, Graduate School of Engineering, Kyoto University, Kyoto 615-8510, Japan
[2] Faculty of Agriculture, Meijo University, 1-501 Shiogamaguchi, Tenpaku, Nagoya 468-8502, Japan
[3] Department of Chemistry, Graduate School of Science, Kobe University, Nada, Kobe, Hyogo 657-8501, Japan

[a)] **Author to whom correspondence should be addressed:** hashimoto.kota.27z@kyoto-u.jp

ABSTRACT

Atomic force microscopy can observe structures of liquids (solvents) on solid surfaces as oscillating force curves. The oscillation originates from the solvation force, which is affected by the interaction between the probe, substrate, and solvents. To investigate the effects of the interactions on the force curve, we calculated the force curves by integral equation theory with various probe and substrate conditions. The probe solvophilicity affected the force curves more than the substrate solvophilicity in our calculation, and its reason is qualitatively explained by the amount of the desolvated solvents. We evaluated the probes and parameters in terms of the qualitative estimation of the number density distribution of the solvent on the wall. The negative of the force curve's derivative with respect to the surface separation reflected the number density distribution better than the force curve. This parameter is based on the method that is proposed previously by Amano *et al.* [Phys. Chem. Chem. Phys. **18**, 15534 (2016)]. The normalized frequency shift can also be used for the qualitative estimation of the number density distribution if the cantilever amplitude is small. Solvophobic probes reflected the number density distribution better than the solvophilic probes. Solvophilic probes resulted in larger oscillation amplitudes than solvophobic probes and are suitable for measurements with a high S/N ratio.

INTRODUCTION

Liquids are isotropic in bulk but not at interfaces. Liquid molecules often form layer structures at solid–liquid interfaces where the number density distribution in the normal direction has the shape of a damped oscillation. These layer structures are very important, e.g., water molecules on biomembranes are crucial for biomolecular functions at the membrane.[1] In addition, the behaviors of lubricant molecules are important to understand and control the friction at the boundary lubrication conditions.[2] Developing experimental methods that enable us to observe the structure of liquid molecules at the solid–liquid interface is important for the understanding of these subjects.

Structures of liquid molecules at solid–liquid interfaces are observed by x-ray and neutron reflectivity measurements,[3–5] surface force apparatus (SFA),[6–8] and atomic force microscopy (AFM).[9–11] AFM does not require synchrotron facilities as reflectivity measurements, and it can treat various types of substrates compared to SFA. In AFM, the force between the probe and the substrate can be measured, and the force plotted against the probe–substrate distance is called the "force curve." The force curve reflects the solvation structure formed on the substrate, and it takes the shape of a damped oscillation if there is a layer structure. Since the force induced by the liquid structure confined between the probe and the substrate is very small, FM-AFM[12] (frequency modulated AFM) is used for the observation of layer structure, which has high force and spatial resolutions. In FM-AFM, the tip is oscillated with a constant amplitude and the frequency shift is recorded. The frequency shift is converted to force through analytical expressions.[13] The oscillatory frequency shift is also regarded as the proof of the layer structure. Oscillatory

force curves and frequency shifts are observed with many liquids such as water,[10,14–19] octamethylcyclotetrasiloxane,[9,20] dodecanol,[21] and alkanes.[22,23]

The force curve quantitatively reflects the number density distribution of the solvent molecules near the substrate (i.e., the solvation structure), but the actual relationship is not clear. Principally, the number density distribution is affected by the bulk number density, the solvent–solvent pair potential, and the substrate–solvent pair potential. The force curve is also affected by them and further by the probe–solvent pair potential and the probe–substrate pair potential. There are some methods to convert the force curve to the number density distribution.[24–27]

Solvent tip approximation (STA)[24,25] treats the probe as a solvent molecule. This approximation is derived from the assumption that the force acting on the apex of the probe is meditated through a single solvent molecule adsorbed on the apex. This method is very simple, but the result does not reflect the probe character. Extensions of STA are proposed, which include the effect of the detailed solvation structure around the probe calculated from molecular dynamics simulations.[28,29] However, they focus on calculating the force curve from the number density distribution, and it is difficult to calculate the number density distribution from the force curve using those methods.

Hemispherical probe approximation (HPA)[26] treats the probe tip as a hemisphere and assumes that the probe–solvent pair potential is a rigid potential. This method includes the effect of the probe size, but the rigid potential assumption causes errors in the number density distribution when the actual potential is far from the rigid one. Hashimoto *et al.* developed a method that assumes that the probe–particle and substrate–particle pair potentials are the same but can be arbitrary.[27] This condition is achievable when the particle is a colloidal particle, but it is hard to satisfy the assumption when the particle is a solvent molecule. All the methods require that the solvent molecule is spherical.

The quantitative calculation of the number density distribution from the force curve is difficult because it is hard to know about the character of the probe tip. However, it is possible to compare the relative change in the force curve when changing the conditions while using the same probe. In this study, we investigate how the number density distribution and the force curve change when changing the solvent, substrate, and probe.

We use numerical calculations based on integral equation theory,[30] which provides force curves with short computation time. Molecular dynamics (MD) simulation is widely used for calculating the distributions[19] and force curves[31–33] from the pair potentials. However, MD simulation needs long calculation time to calculate the potentials of mean force. When the solvents are confined between the probe and the substrate, it takes a longer time due to the decrease in the diffusion coefficient. Integral equation theory can calculate the potentials of mean force quickly with no statistical error, so it is suited for calculating at various conditions. Solvation forces and AFM force curves are calculated using theoretical methods such as integral equation theory[34] and classical density functional theory.[35] Karanikas *et al.*[36] calculated the solvation forces between two flat walls changing the attraction/repulsion between the solvent–solvent and substrate–solvent. Amano *et al.*[25] calculated the number density distributions on a molecular substrate, changing the strength of the attraction between the solvent–probe and substrate–probe. They also calculated the force curves and showed the reconstructed number density distributions from the force curves using STA. Our study works on the comparison of the probe conditions in terms of the similarity of the number density distribution and the force curve changes when changing the solvent and substrate conditions. This evaluation will clarify what kind of probe is suitable for experiments.

THEORY

In the present study, we use reference interaction site model (RISM)[37] theory, which is one of the integral equation theories for molecular liquids. In RISM theory, a molecule is treated as a set of interaction sites. Each interaction site has spherical symmetry. The vibration and the bending of the bonds are difficult to incorporate in the calculation, so the molecule is treated as rigid. We note that the flexible model and the rigid model of hard-dumbbells,[38] H_2O,[39] and CO_2[40] have very similar radial distribution functions.

Two equations are needed for the RISM calculation. The first one is the RISM equation,

$$\rho_\alpha\rho_\gamma\tilde{h}_{\alpha\gamma}(k) = \sum_\mu\sum_\nu \rho_\alpha\tilde{\omega}_{\alpha\mu}(k)\tilde{c}_{\mu\nu}(k)\left(\rho_\gamma\tilde{\omega}_{\nu\gamma}(k) + \rho_\nu\rho_\gamma\tilde{h}_{\nu\gamma}(k)\right), \quad (1)$$

where h is the total correlation function, ω is the intramolecular correlation function, c is the direct correlation function, and ρ is the bulk number density of the molecule. Σ is the summation among all sites. The tilde symbol $\tilde{X}$ is the spherical symmetric Fourier transform of a function X,

$$\tilde{X}(k) = \frac{4\pi}{k}\int_0^\infty dr\, rX(r)\sin(kr). \quad (2)$$

Here, r is the intermolecular center–center distance between the sites and k is the inverse intermolecular center–center distance between the sites. The subscripts of the functions indicate the interaction sites, for example, $\tilde{h}_{\alpha\gamma}$ represents the Fourier transform of the total correlation function between sites α and γ. ρ_α is the bulk number density of the molecule, which contains site α. ω can be written as

$$\tilde{\omega}_{\alpha\gamma}(k) = \begin{cases} 1 & (\alpha = \gamma) \\ \frac{\sin(L_{\alpha\gamma}k)}{L_{\alpha\gamma}k} & (\alpha \neq \gamma,\ \alpha \text{ and } \gamma \text{ are in the same molecule}) \\ 0 & (\alpha \neq \gamma,\ \alpha \text{ and } \gamma \text{ are not in the same molecule}), \end{cases} \quad (3)$$

where $L_{\alpha\gamma}$ is the intramolecular distance between site α and site γ.

The second one is the closure equation. We use the Kovalenko–Hirata closure (KH)[41] in the present study,

$$h_{\alpha\gamma}(r) = \begin{cases} \exp(-\beta u_{\alpha\gamma}(r) + h_{\alpha\gamma}(r) - c_{\alpha\gamma}(r)) - 1 & (h_{\alpha\gamma}(r) \leq 0) \\ -\beta u_{\alpha\gamma}(r) + h_{\alpha\gamma}(r) - c_{\alpha\gamma}(r) & (h_{\alpha\gamma}(r) > 0), \end{cases} \quad (4)$$

where $\beta = 1/k_BT$ is the inverse temperature, k_B is the Boltzmann constant, T is the absolute temperature, and u is the pair potential. The advantage of the KH is that it does not produce negative density distributions, and the calculation is less likely to diverge.[42]

By using Eqs. (1) and (4), we can obtain all hs and cs from us, ωs, ρ, and T. The radial distribution function g can be calculated from h,

$$g_{\alpha\gamma}(r) = h_{\alpha\gamma}(r) + 1. \tag{5}$$

The potential of mean force w (the potential including the effect of the other surrounding molecules) can be calculated from g,

$$-\beta w_{\alpha\gamma}(r) = \ln(g_{\alpha\gamma}(r)). \tag{6}$$

We treat the AFM probe and the substrate wall as spherical solutes. When two types of solutes, wall (W) and probe (P), are immersed in the solvent, the correlation functions between W, P, and the solvent sites can be expressed as

$$\tilde{h}_{W\alpha}(k) = \sum_{\nu} \tilde{c}_{W\nu}(k)\left(\tilde{\omega}_{\nu\alpha}(k) + \rho\tilde{h}_{\nu\alpha}(k)\right), \tag{7}$$

$$\tilde{h}_{P\alpha}(k) = \sum_{\nu} \tilde{c}_{P\nu}(k)\left(\tilde{\omega}_{\nu\alpha}(k) + \rho\tilde{h}_{\nu\alpha}(k)\right), \tag{8}$$

$$\tilde{h}_{WP}(k) = \tilde{c}_{WP}(k) + \rho\sum_{\nu} \tilde{c}_{W\nu}(k)\tilde{h}_{\nu P}(k), \tag{9}$$

where ρ with no subscript is the bulk number density of the solvents and Σ is the summation among the sites of the solvents. The force curve f_{WP} can be calculated by

$$f_{WP}(r) = -\frac{dw_{WP}(r)}{dr} = \frac{1}{\beta}\frac{d\ln(g_{WP}(r))}{dr}. \tag{10}$$

We examine two parameters other than the force curve. The first one is the potential of mean force. Kimura *et al.*[43] derived a proportional relation between the force curve and the normalized number density distribution by assuming that the probe–solvent pair potential is a delta function,

$$f_{WP}(r_{WP}) \propto -\frac{dg_{WS}(r_{WP})}{dr_{WP}}, \tag{11}$$

where r_{WP} is the distance between the wall and the probe. By integrating and multiplying −1 on both sides, we obtain

$$w_{WP}(r_{WP}) \propto g_{WS}(r_{WP}) - 1 = h_{WS}(r_{WP}), \tag{12}$$

where w_{WP} is the potential of mean force between the wall and the probe (hereinafter called PMF). The term −1 appears from $g_{WS}(\infty) = 1$. Hereinafter, we call this relation as delta probe approximation (DPA).

The second parameter is the pressure between two flat walls. This is based on HPA,[26] which is a method to transform the force curve to the number density distribution. HPA is expressed as

$$g_{WS}(r_{WS}) = \frac{\beta P\left(r_{WS} + \frac{\sigma_S}{2} - \frac{\sigma_W}{2}\right)}{\rho g_{Pcp}} + 1, \tag{13}$$

where r_{WS} is the center–center distance between the (spherical) wall and solvent, $P(l)$ is the pressure between two flat walls when the surface separation is l, and g_{Pcp} is the normalized contact number density on the probe. The two flat walls correspond to the probe and wall sphere. We note that the definition of l is different from that in Ref. 26, and we do not use the "patch method" in Ref. 26.

It is hard to determine g_{Pcp} because the probe–solvent pair potential is not the hard wall potential in our calculation. If we ignore the proportionality coefficients,[44]

$$g_{WS}(r_{WS}) - 1 = h_{WS}(r_{WS}) \propto P\left(r_{WS} + \frac{\sigma_S}{2} - \frac{\sigma_W}{2}\right) \tag{14}$$

is obtained. The authors of Ref. 26 used an integral equation to calculate P from f_{WP}, but we use the Derjaguin approximation[45] for simplicity,

$$\frac{d}{dr_{WP}}f_{WP}(r_{WP}) = -2\pi RP\left(r_{WP} - \frac{\sigma_P}{2} - \frac{\sigma_W}{2}\right), \tag{15}$$

where r_{WP} is the center–center distance between the (spherical) wall and probe and R is the "radius of the probe." We note that the Derjaguin approximation becomes accurate when R is large enough than the solvent radius. Combining Eqs. (14) and (15), we obtain

$$h_{WS}(r_{WS}) \propto P\left(r_{WS} + \frac{\sigma_S}{2} - \frac{\sigma_W}{2}\right) \propto -\frac{d}{dr_{WS}}f_{WP}\left(r_{WS} + \frac{\sigma_S}{2} + \frac{\sigma_P}{2}\right). \tag{16}$$

We calculate the PMF w_{WP} (hereinafter called PMF), force curve f_{WP}, and pressure between two flat walls P (hereinafter called pressure) and study which parameter is better for the qualitative estimation of the number density distribution.

CALCULATION

The pair potential between the solvent sites u_{SS} is represented by a 12-6 Lennard-Jones potential,

$$u_{SS}(r) = 4\epsilon_{SS}\left(\left(\frac{\sigma_S}{r}\right)^{12} - \left(\frac{\sigma_S}{r}\right)^{6}\right), \tag{17}$$

where ϵ_{SS} is the depth of the potential and σ_S is the diameter of the site. The solvophilic probe and wall are represented by a shifted 12-6 Lennard-Jones potential,

$$u_{LWS}(r) = \begin{cases} \infty & \left(r < \frac{\sigma_W}{2} - \frac{\sigma_S}{2}\right) \\ 4\epsilon_{WS}\left(\left(\frac{\sigma_S}{r-\frac{\sigma_W}{2}+\frac{\sigma_S}{2}}\right)^{12} - \left(\frac{\sigma_S}{r-\frac{\sigma_W}{2}+\frac{\sigma_S}{2}}\right)^{6}\right) & \left(\frac{\sigma_W}{2} - \frac{\sigma_S}{2} \le r\right), \end{cases} \tag{18}$$

$$u_{LPS}(r) = \begin{cases} \infty & \left(r < \frac{\sigma_P}{2} - \frac{\sigma_S}{2}\right) \\ 4\epsilon_{WS}\left(\left(\frac{\sigma_S}{r-\frac{\sigma_P}{2}+\frac{\sigma_S}{2}}\right)^{12} - \left(\frac{\sigma_S}{r-\frac{\sigma_P}{2}+\frac{\sigma_S}{2}}\right)^{6}\right) & \left(\frac{\sigma_P}{2} - \frac{\sigma_S}{2} \le r\right), \end{cases} \tag{19}$$

where ϵ_{WS} and ϵ_{PS} are the depths of the potential and σ_W and σ_P are the diameters of the wall and the probe, respectively. We call the solvophilic wall and probe LW (Like Wall) and LP (Like Probe), respectively. For the solvophobic probe and wall, we use a shifted and truncated 12-6 Lennard-Jones potential,

$$u_{\mathrm{DWS}}(r) = \begin{cases} \infty & \left(r < \frac{\sigma_W}{2} - \frac{\sigma_S}{2}\right) \\ 4\epsilon_{WS}\left(\left(\frac{\sigma_S}{r-\frac{\sigma_W}{2}+\frac{\sigma_S}{2}}\right)^{12} - \left(\frac{\sigma_S}{r-\frac{\sigma_W}{2}+\frac{\sigma_S}{2}}\right)^{6}\right) + \epsilon_{WS} & \left(\frac{\sigma_W}{2} - \frac{\sigma_S}{2} \le r < \frac{\sigma_W}{2} - \frac{\sigma_S}{2} + 2^{\frac{1}{6}}\sigma_S\right) \\ 0 & \left(\frac{\sigma_W}{2} - \frac{\sigma_S}{2} + 2^{\frac{1}{6}}\sigma_S \le r\right), \end{cases} \tag{20}$$

$$u_{\mathrm{DPS}}(r) = \begin{cases} \infty & \left(r < \frac{\sigma_P}{2} - \frac{\sigma_S}{2}\right) \\ 4\epsilon_{PS}\left(\left(\frac{\sigma_S}{r-\frac{\sigma_P}{2}+\frac{\sigma_S}{2}}\right)^{12} - \left(\frac{\sigma_S}{r-\frac{\sigma_P}{2}+\frac{\sigma_S}{2}}\right)^{6}\right) + \epsilon_{PS} & \left(\frac{\sigma_P}{2} - \frac{\sigma_S}{2} \le r < \frac{\sigma_P}{2} - \frac{\sigma_S}{2} + 2^{\frac{1}{6}}\sigma_S\right) \\ 0 & \left(\frac{\sigma_P}{2} - \frac{\sigma_S}{2} + 2^{\frac{1}{6}}\sigma_S \le r\right). \end{cases} \tag{21}$$

We call the solvophobic wall and probe DW (Dislike Wall) and DP (Dislike Probe), respectively. Usually, a 9-3 Lennard-Jones potential is used for dispersion force of aggregation of atoms, but we chose 12-6 for simplicity. LW and LP will be more solvophilic if 9-3 is used because 9-3 decays slower than 12-6. However, the relative values of the results should not significantly change. Figure 1 shows the pair potentials used in the calculation. $\sigma_S^{\mathrm{eff}} = 2^{\frac{1}{6}}\sigma_S$ is defined as the effective diameter, which is the position of the potential minimum at the like potential. In this study, we focus on the effects of the solvents. Thus, the pair potentials between the wall and probe are set to a rigid potential.

We fix σ_S = 5 Å, σ_W = 150 Å, and $\epsilon_{SS} = \epsilon_{WS} = \epsilon_{PS} = k_B T$. σ_W is large enough to compare the trends of force curves (see Fig. S1). Three types of solvents, O (1O), OO (2O), and OOO (3O), are prepared, where O represents a site with diameter σ_S. The distance between the centers of the interaction sites is 5 Å. The three sites of 3O are lined up in a row. The bulk number densities of 1O, 2O, and 3O are 10.00, 5.430, and 3.735 mol/l, respectively. These values are chosen to match the pressure of the solvents. Their volume fractions calculated from the effective diameter σ_S^{eff} are 56%, 60%, and 62%, respectively.

The conditions we changed among the calculations are the solvent type (1O/2O/3O), wall type (LW/DW), probe type (LP/DP), and probe diameter σ_P. Figure 2 shows the solvent, probe, and wall used in the calculation. The number before LP and DP represents σ_P/Å. For example, a solvophobic probe with a diameter of σ_P = 10 Å is called 10DP.

We use $R = \frac{\sigma_P}{2} - \frac{\sigma_S}{2} + 2^{\frac{1}{6}}\sigma_S$ instead of $R = \sigma_P/2$ in Eq. (15) because the forces induced on the probe are exerted from the sphere, which is composed of the centers of the contacting solvent sites.[26,46] If $R = \sigma_P/2$ is used, f_{WP} becomes 0 at $\sigma_P = 0$. However, there should be non-zero force because the excluded volume remains at $\sigma_P = 0$. $\frac{\sigma_P}{2} - \frac{\sigma_S}{2} + 2^{\frac{1}{6}}\sigma_S$ is the distance at the potential minimum in Eq. (19) and the 0 potential in Eq. (21).

The grid interval is 0.05 Å. The number of grid points is 16384. We used the calculation software rism1d, which we modified to input arbitrary potentials. The original rism1d is contained in AmberTools18.[47]

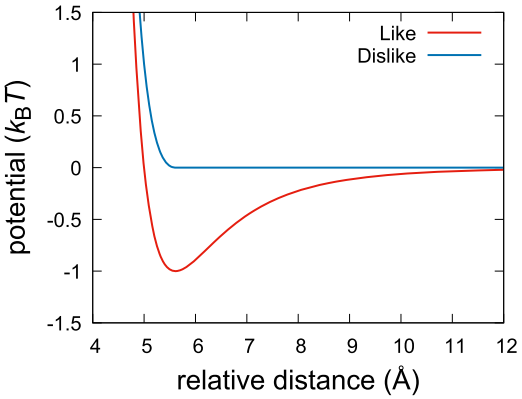

FIG. 1. Pair potential used in the calculation. The actual distance depends on the radius of the elements.

RESULT AND DISCUSSION

Figure 3 shows the normalized number density distribution g_{WS}. Table I lists the conditions and the legends used in Fig. 3. g_{WS}'s of edge O, center O, and total of them in 3O are labeled "-E," "-C," and "-EC," respectively. The distance (x-axis) is defined as $r - \frac{\sigma_W}{2}$. The first peaks on LW [Fig. 3(a)] are higher than those on DW for the corresponding conditions [Fig. 3(b)] because of the attraction between the wall and the solvent. As the number of sites in the solvent increases from 1O to 2O and 3O, the first peak decreases and the second peak slightly decreases. The effects of the solvent type are smaller than the effects of the wall type [Fig. 3(c)]. When the solvent

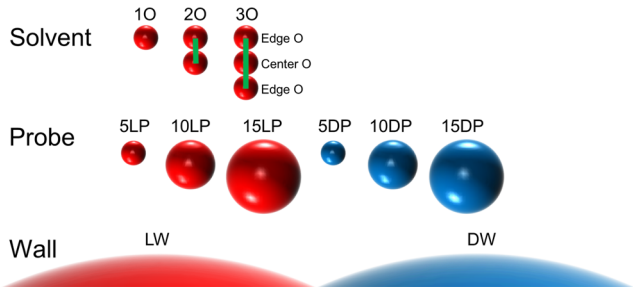

FIG. 2. Illustrations of the solvent, probe, and wall used in the calculation.

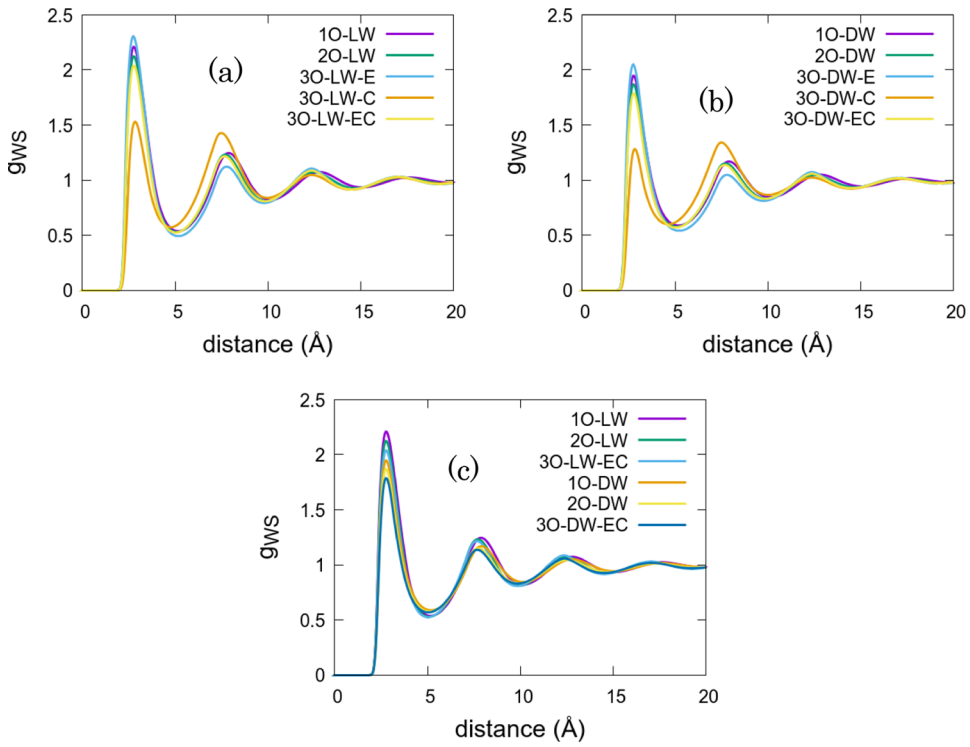

FIG. 3. Normalized number density distribution of the solvents on the wall. (a) Solvophilic wall, (b) solvophobic wall, and (c) all conditions excluding 3O-LW-E, 3O-LW-C, 3O-DW-E, and 3O-DW-C.

type is 3O, the first peak of center O corresponds to the 3O lying on the wall. The first peak of edge O corresponds to the 3O lying, standing, or tilting. The ratios of the lying 3Os to the lying, standing, or tilting 3Os at the first layer are 55% on LW and 52% on DW. The ratios of the O sites in the lying 3Os to all the Os in the first layer are 79% on LW and 77% on DW. The ratio of 3Os, which are tilting, should be small because the center O g_{WS} between the first layer and the second layer is small.

Figure 4 compares the PMFs and force curves and pressures with different solvent types (1O/2O/3O), wall types (LW/DW), and probe types (LP/DP). The surface separation (x-axis) is defined as $r - \frac{\sigma_W}{2} - \frac{\sigma_P}{2}$. Table II lists the conditions and the legends used in Fig. 4. The jump around the surface separation distance of 1 Å in Fig. 4(e) originates from the KH closure. All the PMFs, force curves, and pressures have the same oscillation length, and it is close to the solvent site diameter σ_S.

TABLE I. Conditions for the number density distributions in Fig. 3.

Name	Solvent	Wall	Target solvent
1O-LW	1O	L	...
2O-LW	2O	L	...
3O-LW-E	3O	L	Edge O
3O-LW-C	3O	L	Center O
3O-LW-EC	3O	L	Edge O and center O
1O-DW	1O	D	...
2O-DW	2O	D	...
3O-DW-E	3O	D	Edge O
3O-DW-C	3O	D	Center O
3O-DW-EC	3O	D	Edge O and center O

The major factor affecting the PMFs, force curves, and pressures is the probe type. DP "dislikes" the solvents, so the PMF decreases as it becomes close to the wall. LP "likes" the solvents (as other solvents), so the PMF does not decrease as the PMF of DP. The same effect goes with LW and DW, but the effect is small.

Intuitively, the effect of the wall seems to be larger than the probe because the surface of the wall is larger than that of the probe. The reason can be qualitatively explained as follows (see Fig. 5). The PMF is mainly determined by the first solvent layer on the wall or the probe [see the red lines in Figs. 5(a) and 5(b)]. This is because the pair potential is close to 0 in the second layer and the further ones. When the wall and the probe contacts, the first layer on the wall/probe is excluded by the probe/wall [see the green lines in Figs. 5(c) and 5(d)]. The area of the excluded first layer on the probe is larger than the area of the excluded first layer on the wall [compare the length of the green lines of Figs. 5(c) and 5(d). The relation in the line length is the same as that in the area]. The desolvated area around the probe is larger than the wall, even when the probe size is larger than the solvent. Thus, the effect of the first layer on the probe is larger than the effect of the first layer on the wall. The type (solvophilic/solvophobic) of the probe and the wall affects the number density of the first layer. Therefore, the effect of the probe type is larger than that of the wall type. Since we use simple pair potentials, we cannot conclude immediately that the probe solvophilicity affects the force curve more strongly than the substrate

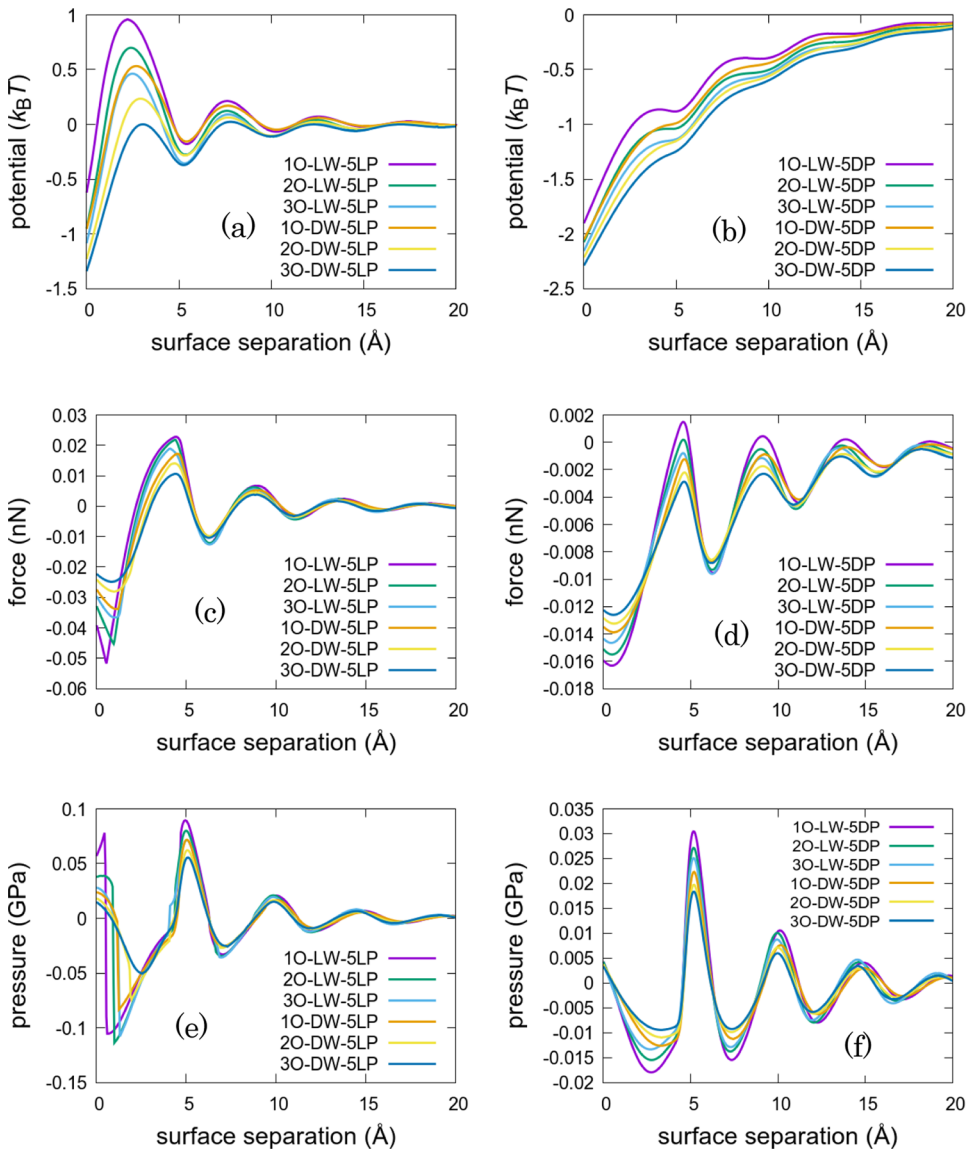

FIG. 4. PMFs, force curves, and pressures with different solvent, wall, and probe types. The conditions are listed in Table II. [(a) and (b)] PMF between the wall and probe. [(c) and (d)] Force curve between the wall and probe. [(e) and (f)] Pressure between two flat walls. [(a), (c), and (e)] Solvophilic probe. [(b), (d), and (f)] Solvophobic probe.

solvophilicity in the actual experiments. However, the results suggest that the probe type effect can be as large as the substrate type effect in general.

Kaggwa *et al.*[14] measured force curves in water with hydrophilic and hydrophobic probes and hydrophilic and hydrophobic substrates. The hydrophilic probe and hydrophilic substrate were both oxidized silicon, and the hydrophobic probe and hydrophobic substrate were both hydrophobized by hexamethyldisilazane. Since the hydrophilicity and the hydrophobicity of the probes and the substrates are almost the same, the effect of the probe should be larger than the substrate according to our calculation. On the contrary, the force curves with the hydrophilic substrate showed oscillations, whereas the force curves with the hydrophobic substrate showed no oscillations. The probe type did not affect the existence of the oscillation, which means that the substrate type effect is larger than the probe type effect. The difference between our calculation and the experiment might originate from the characteristics of water such as the long-range electrostatic interactions and the anisotropy of the hydrogen bond, both of which are not included in our calculation. Unfortunately, to our knowledge, the comparison of force curves with solvophilic and solvophobic probes and substrates in nonpolar liquids is not performed, but we expect that the experimental result will agree with our calculation. As a side note, oscillatory frequency shifts are reported with other hydrophobic substrates in water.[15–19]

The effect of the solvent type is simple (Fig. 4). The PMFs decrease as the number of spheres per molecule increases. As the number of spheres per molecule increases, the restriction on the

TABLE II. Conditions for the PMFs, force curves, and pressures in Fig. 4. The other condition is σ_P = 5 Å.

Name	Solvent	Wall	Probe
1O-LW-5LP	1O	L	L
2O-LW-5LP	2O	L	L
3O-LW-5LP	3O	L	L
1O-LW-5DP	1O	L	D
2O-LW-5DP	2O	L	D
3O-LW-5DP	3O	L	D
1O-DW-5LP	1O	D	L
2O-DW-5LP	2O	D	L
3O-DW-5LP	3O	D	L
1O-DW-5DP	1O	D	D
2O-DW-5DP	2O	D	D
3O-DW-5DP	3O	D	D

configuration of the spheres increases. 2O and 3O have configuration restrictions in addition compared to 1O. The O sites in the solvents become hard to take the optimal configuration on the wall and the spheres, so the wall and the probe become solvophobic, and the PMF decreases. The third peaks of the 3O PMFs, force curves, and pressures are not especially high. Experimental AFM force curves in alkanes[22,23] also only show oscillations with the period of the alkane thickness. Actually, nearly 50% of 3Os in the first layer are not lying against the wall. This indicates that even if the PMF, force curve, or pressure does not have features with the solvent length (such as a relatively high peak with the interval of the solvent length), it does not mean that most of the solvents are lying. In a surfactant solution, a peak with the width of the surfactant layer thickness is observed.[23]

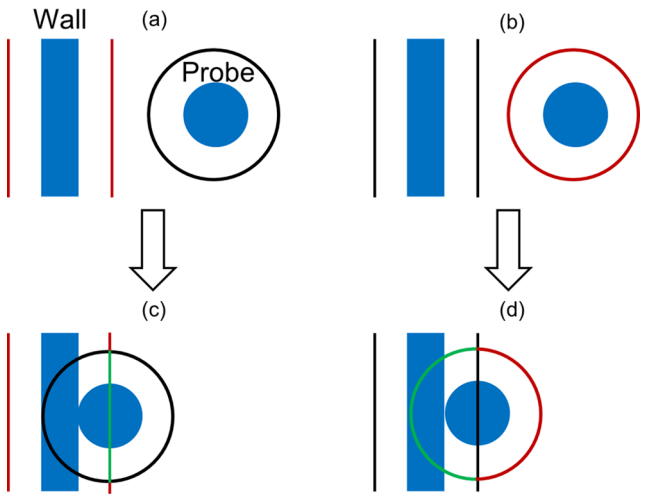

FIG. 5. Schematics of the effect of the first layer of the solvent on the wall and the probe. The black lines show the excluded volume. The red lines indicate the first layer of the solvents. The green lines show the desolvated solvents as the wall–probe contact. [(a) and (c)] The first layer solvents on the wall are desolvated by the probe. [(b) and (d)] The first layer solvents around the probe are desolvated by the wall.

Thus, if almost all of the solvents are standing, it should show a force curve with a feature at the solvent length.

The amplitudes of the PMFs, force curves, and pressures decrease as changing LW to DW (Fig. 4). The amplitude of the PMFs, force curves, and pressures decreases as the number of spheres per molecule increases. These trends are the same as the trend with g_{WS} (Fig. 3). These observations indicate that the PMFs, force curves, and pressures can qualitatively show the trend of g_{WS}.

Figure 6 compares the PMFs, force curves, and pressures with different probe sizes. Table III lists the conditions and the legends used in Fig. 6. The results of 2O and 3O are omitted because the trend did not change from the results of 1O (see Fig. S2 for their results). As the probe size increases, the PMFs and the force curves decrease, and the oscillation amplitudes of the PMFs, force curves, and pressures decrease. This trend is similar to the trend when changing the probe type from LP to DP and indicates that the probe becomes solvophobic as the probe size increases. In this study, u_{LPS} is a simple shifted LJ potential, so this does not suggest that solutes will become solvophobic when their radius becomes large in general.

If the Derjaguin approximation were exact, the pressures with the same conditions other than the probe size should have overlapped. However, the curves do not overlap, and they are not even close to each other [Figs. 6(e) and 6(f)]. As the probe size increases, the amplitude decreases in the PMFs and force curves, although it should increase in the Derjaguin approximation. This results in large amplitude differences in the pressures. In addition, the PMFs and the force curves of 5LP oscillate around 0, but the PMFs and the force curves of 10LP and 15LP have a decreasing trend. The Derjaguin approximation only multiplies by a constant factor, so it cannot deal with the decreasing trend. In conclusion, the Derjaguin approximation fails to calculate the absolute value of the pressures in these conditions. We will show below that the relative values of the pressure are likely to be accurate when comparing the pressures among the same probes. At least, Figs. 4(e), 4(f), 6(e), and 6(f) should not be used to discuss the absolute value of the pressure. The Derjaguin approximation assumes that the pressure between the surface element of the sphere and the surface element of the wall is determined only by the distance between the two surface elements. Actually, the pressure changes if the solvophilicity of the probe changes even if the surface element distance is the same.

We compare the probe types and the probe sizes in terms of the qualitative estimation of the number density distribution. The prediction power of the PMF, force curve, and pressure as the parameter for estimating of the number density distributions is also compared. We focus on how the first peak height and the second peak height change as the wall and the solvent change. If the PMF's, force curve's, or pressure's peak heights change in the same way as the number density distribution's peak heights change when the wall or the solvent changes, the used probe is a good probe. The similarity of the peak height change between the PMF, force curve, and pressure with a certain probe and the number density distribution is evaluated by the following process. The first peak heights of g_{WS}'s are Z-score normalized among all solvent and wall types, which are denoted as $GF_{cond.}$, where *cond.* is the type of the wall and the solvent (1O-LW, 2O-LW, 3O-LW, 1O-DW, 2O-DW, or 3O-DW). $GS_{cond.}$'s are calculated from the second peaks. The same procedure is performed among all *p.t.*'s, and $FF^{p.t.}_{cond.}$'s are calculated from the first peaks and

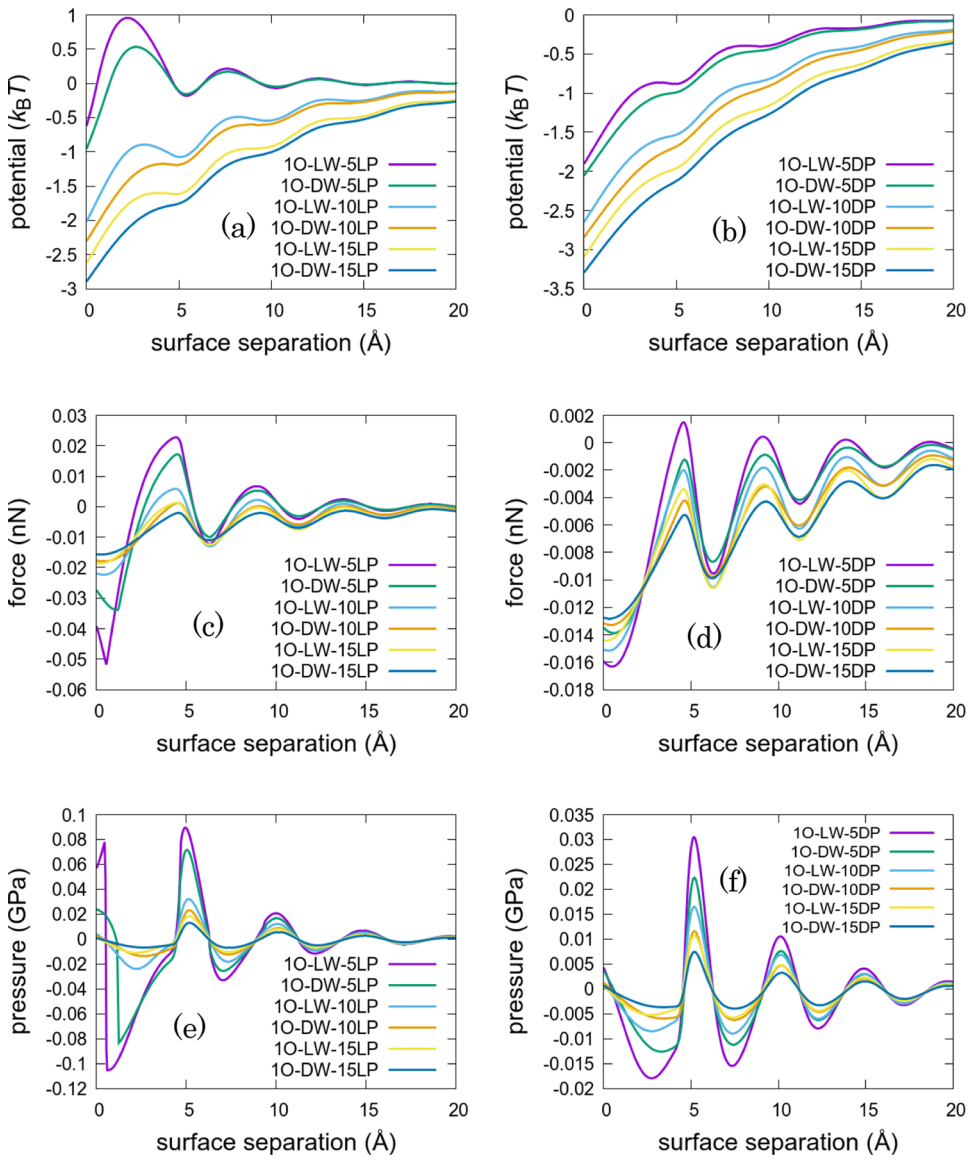

FIG. 6. PMFs, force curves, and pressures with various wall and probe types and probe sizes. The conditions are listed in Table III. (a) and (b) PMF between the wall and probe. (c) and (d) Force curve between the wall and probe. (e) and (f) Pressure between two flat walls. (a), (c), and (e) Solvophilic probe. (b), (d), and (f) Solvophobic probe.

$FS^{p.t.}_{cond.}$'s are calculated from the second peaks, where *p.t.* is the combination of the probe type and size (5LP, 5DP, 10LP, 10DP, 15LP, or 15DP) and the parameter type (PMF, FC, or PS, where FC is the force curve and PS is the pressure). To summarize, the options of *p.t.* are 5LP-PMF, 5DP-PMF, 10LP-PMF, 10DP-PMF, 15LP-PMF, 15DP-PMF, 5LP-FC, 5DP-FC, 10LP-FC, 10DP-FC, 15LP-FC, 15DP-FC, 5LP-PS, 5DP-PS, 10LP-PS, 10DP-PS, 15LP-PS, and 15DP-PS. The Euclidean distance $LF^{p.t.}$ between $FF^{p.t.}_{cond.}$ and $GF^{p.t.}_{cond.}$ is calculated by

$$LF^{p.t.} = \sqrt{\sum_{cond.} \left(FF^{p.t.}_{cond.} - GF_{cond.}\right)^2}. \tag{22}$$

$LS^{p.t.}$ is calculated in the same way,

$$LS^{p.t.} = \sqrt{\sum_{cond.} \left(FS^{p.t.}_{cond.} - GS_{cond.}\right)^2}. \tag{23}$$

$LF^{p.t.} + LS^{p.t.}$ is the total probe score. The smaller the score is, the closer the peak changes in the parameter and the number density distribution peak changes are. In other words, the probe with a small score is a good probe. Many PMFs do not have a peak as a maximum. We defined the position of the peak as the minimum of the second derivative (proportional to the pressure) for PMFs except for the PMFs from the 5LP probe. The peaks of 5LP use the usual PMF maxima because they have clear maxima in the PMFs. The jumps in

TABLE III. Conditions for the PMFs, force curves, and pressures in Fig. 6. The other condition is as follows: The solvent type is 1O.

Name	Probe size (σ_P)	Wall	Probe
1O-LW-5LP	5	L	L
1O-LW-10LP	10	L	L
1O-LW-15LP	15	L	L
1O-LW-5DP	5	L	D
1O-LW-10DP	10	L	D
1O-LW-15DP	15	L	D
1O-DW-5LP	5	D	L
1O-DW-10LP	10	D	L
1O-DW-15LP	15	D	L
1O-DW-5DP	5	D	D
1O-DW-10DP	10	D	D
1O-DW-15DP	15	D	D

the pressures near the zero surface separation are not counted as the first peaks. The PMFs, force curves, and pressures used for this comparison are shown in Fig. S3. $GF_{cond.}$'s for all conditions are listed in Table S3. $FF^{p.t.}_{cond.}$'s and $FS^{p.t.}_{cond.}$'s for all conditions are listed in Tables S4 and S5, respectively.

Table IV lists the calculated scores. The order of the scores is PMF > FC > PS, so pressure is the best parameter to estimate the number density distribution. HPA claims that the pressure is proportional to the total correlation function [Eq. (14)]. HPA assumes that the probe–solvent pair potential is the hard wall potential and the solvent is spherical. The proportionality coefficient is ignored in our comparison, and this might be the reason that the scores of the pressures were good even though the assumptions are not fulfilled.

TABLE IV. Comparison of the probe scores. -PMF indicates the PMF, -FC indicates the force curve, and -PS indicates the pressure.

Probe type and PMF or FC or PS ($p.t.$)	First peak score ($LF^{p.t.}$)	Second peak score ($LS^{p.t.}$)	Total score ($LF^{p.t.} + LS^{p.t.}$)
5LP-PMF	0.60	1.77	2.37
5DP-PMF	1.51	1.68	3.18
10LP-PMF	1.25	1.82	3.07
10DP-PMF	1.78	1.76	3.54
15LP-PMF	1.43	1.83	3.26
15DP-PMF	1.84	1.84	3.68
5LP-FC	0.38	0.61	0.99
5DP-FC	0.31	1.07	1.38
10LP-FC	0.63	1.27	1.90
10DP-FC	0.37	1.18	1.55
15LP-FC	0.59	1.27	1.87
15DP-FC	0.37	1.16	1.53
5LP-PS	0.46	0.35	0.82
5DP-PS	0.21	0.41	0.62
10LP-PS	0.56	0.78	1.34
10DP-PS	0.40	0.80	1.20
15LP-PS	0.61	0.96	1.57
15DP-PS	0.49	0.97	1.45

We concluded that the Derjaguin approximation does not work in our conditions from Fig. 6. We used the Derjaguin approximation to obtain pressures, but the scores of the pressures were good. The scores are calculated from the relative peak heights with the same probe size. The peak heights between the different probe sizes are not directly compared. The Derjaguin approximation fails to calculate the actual pressure between two flat walls, but the relative peak heights with the same probe size might be accurate.

The scores do not change even if the negative of the force curve's derivative ($-\frac{d}{dr_{WP}} f_{WP}$) is used instead of the pressures. Using the negative of the force curve's derivative will be the simplest method to qualitatively estimate the number density distribution. This method only requires the force curve, and no other parameters are needed.

Sader and Jarvis showed that in the small cantilever amplitude limit, the force curve becomes the integration of the frequency shift normalized by the unperturbed frequency[13] in FM-AFM. By taking the derivative, the normalized frequency shift is proportional to the negative of the force curve's derivative. Thus, if the cantilever amplitude is small, the normalized frequency shift can also be used for the qualitative estimation of the number density distribution.

The scores of PMF are worse than those of the force curve. In DPA, the existence of the probe does not affect the number density distribution of the solvent around the probe. However, since the probe size is the same or larger than the solvent sites, the probe largely affects the number density distribution around the probe. This difference can be considered as the reason of the large score.

STA[24,25] relates the PMF w_{WP} and the normalized number density distribution g_{WS} by

$$g_{WS}(r) = \exp(-\beta w_{WP}(r)). \tag{24}$$

STA is strict when the probe and the solvent are the same ($g_{WS} = g_{WP}$). In STA, the minima of PMF correspond to the number density distribution maxima. We do not show the scores using STA because the scores are very high. The PMF minima decrease as the number of spheres per molecule increases (Fig. 4). Since the number density distribution maxima decrease as the number of spheres per molecule increases, the PMF minima should increase in STA. This shows that STA breaks down largely when the solvent types are different from the probe.

As the probe size increases, the scores of the pressures become worse. This indicates that the probe size should be close to the solvent sphere size. The solvophobic probes have better scores than the solvophilic probes. The solvophobic probes do not have attractions with the solvents, and the probe–solvent pair potential is closer to the hard wall potential than the solvophilic probe. The solvophobic probe fulfills the assumption of HPA better than the solvophilic probe. This makes the score of the solvophobic probe better than the solvophilic probe.

The amplitudes of the PMFs, force curves, and pressures of LP are larger than that of DP. As the probe size increases, the amplitudes of the PMFs, force curves, and pressures decrease. Thus, using a solvophilic and small probe should improve the signal to noise (S/N) ratio in experiments.

Since the wavelengths of the graphs are roughly σ_S, the positions of the maxima move $\frac{\sigma_S}{4}$ when the PMF is changed to the force curve, and the force curve is changed to the pressure. The scores

of the force curves are worse than the pressures, but the differences are not large. It is interesting that the force curves and the pressures produce close results even the surface separation positions corresponding to the number density distribution distance are different.

The first/second peak height ratios of the PMFs, force curves, and pressures are largely different from the number density distributions. The first/second peak height ratio of the 5LP force curve is not so far from the number density distribution, but it is hard to know what probe size in the actual experiment corresponds to the 5 Å probe in this calculation. Therefore, the density ratio of the first layer and the second layer should not be simply discussed from the first and second peak heights.

CONCLUSION

We calculated the number density distributions, PMFs, force curves, and pressures of AFM, changing the solvophilicity of the probes, substrates, and solvent types. The peak heights of the number density distribution were higher on the solvophilic wall compared to the solvophobic wall. As the solvent length increases, the peak heights of the number density distribution decreased. Almost half of the 3O solvents were lying at the substrate wall.

The oscillation lengths of the PMFs, force curves, and pressures were determined by the solvent site diameter and independent of the solvent length. The PMFs, force curves, and pressures of the 3O solvent did not have special features at the third peak even though there were some solvents standing against the substrate wall.

The probe solvophilicity affected the PMFs, force curves, and pressures more strongly than the wall solvophilicity. The reason for this finding was explained by the amount of the desolvated solvents when the probe and wall contact.

The Derjaguin approximation failed largely due to the solvophilicity change in the probe when the probe size changed. According to the Derjaguin approximation, it was expected that the amplitudes of the PMFs and the force curves increase, but they actually decreased. In our calculation, the probe became solvophobic as the probe size increased. This trend is not a universal result because it depends on the pair potential setting, but it suggests that the change in the solvophilicity should be taken into account when using the Derjaguin approximation.

Among the PMF, force curve, and pressure, the pressure reflected the change in the number density distribution the best while changing the solvent and the wall types. The pressure and the total correlation function (normalized number density distribution −1) are proportional under HPA and the Derjaguin approximation. The Derjaguin approximation might be acceptable when comparing the pressure among the results of the same probe sizes. For the qualitative estimation of the number density distribution, the negative of the force curve's derivative, which is proportional to the pressure, is the best and simplest parameter. If the cantilever amplitude is small enough, the normalized frequency shift can also be used for the qualitative estimation of the number density distribution.

The solvophilic probes led to larger amplitudes in the force curves than the solvophobic probes. This means that the usage of a solvophilic probe will increase the S/N ratio in actual experiments. The solvophobic probes reflected the change in the number density distributions better than the solvophilic probe because it fulfills the assumption of HPA better.

SUPPLEMENTARY MATERIAL

The effect of the wall sphere diameter, the effect of the probe sizes with 2O or 3O solvents, and the data of Z-score normalized peak heights are described in the supplementary material.

ACKNOWLEDGMENTS

This work was supported by the Grant-in-Aid for Young Scientists (B) from Japan Society for the Promotion of Science (Grant No. 15K21100) and the Kyoto University Education and Research Foundation. We appreciate the website "Digipot," which provides free images (http://www.digipot.net/).

The authors have no competing interest to declare.

DATA AVAILABILITY

The data that support the findings of this study are available from the corresponding author upon reasonable request.

REFERENCES

[1] E. Schneck, F. Sedlmeier, and R. R. Netz, Proc. Natl. Acad. Sci. U. S. A. **109**, 14405 (2012).
[2] X. Zheng, H. Zhu, B. Kosasih, and A. Kiet Tieu, Wear **301**, 62 (2013).
[3] L. Cheng, P. Fenter, K. L. Nagy, M. L. Schlegel, and N. C. Sturchio, Phys. Rev. Lett. **87**, 156103 (2001).
[4] K. Nygård and O. Konovalov, Soft Matter **8**, 5180 (2012).
[5] M. Bellissent-Funel, R. Sridi-Dorbez, and L. Bosio, J. Chem. Phys. **104**, 10023 (1996).
[6] R. G. Horn and J. N. Israelachvili, J. Chem. Phys. **75**, 1400 (1981).
[7] H. K. Christenson, D. W. R. Gruen, R. G. Horn, and J. N. Israelachvili, J. Chem. Phys. **87**, 1834 (1987).
[8] J. N. Israelachvili and R. M. Pashley, Nature **306**, 249 (1983).
[9] S. J. O'Shea, M. E. Welland, and T. Rayment, Appl. Phys. Lett. **60**, 2356 (1992).
[10] T. Fukuma, Y. Ueda, S. Yoshioka, and H. Asakawa, Phys. Rev. Lett. **104**, 016101 (2010).
[11] T. Hiasa, K. Kimura, and H. Onishi, Colloids Surf., A **396**, 203 (2012).
[12] T. R. Albrecht, P. Grütter, D. Horne, and D. Rugar, J. Appl. Phys. **69**, 668 (1991).
[13] J. E. Sader and S. P. Jarvis, Appl. Phys. Lett. **84**, 1801 (2004).
[14] G. B. Kaggwa, P. C. Nalam, J. I. Kilpatrick, N. D. Spencer, and S. P. Jarvis, Langmuir **28**, 6589 (2012).
[15] I. Schlesinger and U. Sivan, Langmuir **33**, 2485 (2017).
[16] C.-W. Yang, K. Miyazawa, T. Fukuma, K. Miyata, and I.-S. Hwang, Phys. Chem. Chem. Phys. **20**, 23522 (2018).
[17] K. Suzuki, N. Oyabu, K. Kobayashi, K. Matsushige, and H. Yamada, Appl. Phys. Express **4**, 125102 (2011).
[18] T. Utsunomiya, Y. Yokota, T. Enoki, and K. I. Fukui, Chem. Commun. **50**, 15537 (2014).
[19] H. Söngen, Y. Morais Jaques, L. Zivanovic, S. Seibert, R. Bechstein, P. Spijker, H. Onishi, A. S. Foster, and A. Kühnle, Phys. Rev. B **100**, 205410 (2019).
[20] T. Uchihashi, M. Higgins, Y. Nakayama, J. E. Sader, and S. P. Jarvis, Nanotechnology **16**, S49 (2005).
[21] T. Hiasa, K. Kimura, and H. Onishi, J. Phys. Chem. C **116**, 26475 (2012).
[22] D. L. Klein and P. L. McEuen, Appl. Phys. Lett. **66**, 2478 (1995).
[23] T. Hirayama, R. Kawamura, K. Fujino, T. Matsuoka, H. Komiya, and H. Onishi, Langmuir **33**, 10492 (2017).

[24]M. Watkins and B. Reischl, J. Chem. Phys. **138**, 154703 (2013).
[25]K. Amano, K. Suzuki, T. Fukuma, O. Takahashi, and H. Onishi, J. Chem. Phys. **139**, 224710 (2013).
[26]K. Amano, Y. Liang, K. Miyazawa, K. Kobayashi, K. Hashimoto, K. Fukami, N. Nishi, T. Sakka, H. Onishi, and T. Fukuma, Phys. Chem. Chem. Phys. **18**, 15534 (2016).
[27]K. Hashimoto, K. Amano, N. Nishi, and T. Sakka, J. Mol. Liq. **294**, 111584 (2019).
[28]K. Miyazawa, J. Tracey, B. Reischl, P. Spijker, A. S. Foster, A. L. Rohl, and T. Fukuma, Nanoscale **12**, 12856 (2020).
[29]E. Nakouzi, A. G. Stack, S. Kerisit, B. A. Legg, C. J. Mundy, G. K. Schenter, J. Chun, and J. J. De Yoreo, J. Phys. Chem. C **125**, 1282 (2021).
[30]J. P. Hansen and I. R. McDonald, *Theory of Simple Liquids* (Academic Press, 2006).
[31]T. Fukuma, B. Reischl, N. Kobayashi, P. Spijker, F. F. Canova, K. Miyazawa, and A. S. Foster, Phys. Rev. B **92**, 155412 (2015).
[32]M. Watkins, M. L. Berkowitz, and A. L. Shluger, Phys. Chem. Chem. Phys. **13**, 12584 (2011).
[33]R. G. Xu and Y. Lenga, J. Chem. Phys. **140**, 214702 (2014).
[34]M. Harada and M. Tsukada, Phys. Rev. B **82**, 035414 (2010).
[35]J. Hernández-Muñoz, E. Chacón, and P. Tarazona, J. Chem. Phys. **151**, 034701 (2019).
[36]S. Karanikas, J. Dzubiella, A. Moncho-Jordá, and A. A. Louis, J. Chem. Phys. **128**, 204704 (2008).
[37]D. Chandler and H. C. Andersen, J. Chem. Phys. **57**, 1930 (1972).
[38]G. A. Chapela and S. E. Martínez-Casas, Mol. Phys. **50**, 129 (1983).
[39]J. S. Medina, R. Prosmiti, P. Villarreal, G. Delgado-Barrio, G. Winter, B. González, J. V. Alemán, and C. Collado, Chem. Phys. **388**, 9 (2011).
[40]C. G. Aimoli, E. J. Maginn, and C. R. A. Abreu, J. Chem. Phys. **141**, 134101 (2014).
[41]A. Kovalenko, S. Ten-No, and F. Hirata, J. Comput. Chem. **20**, 928 (1999).
[42]*Molecular Theory of Solvation*, edited by F. Hirata (Kluwer Academic Publishers, Dordrecht, 2004).
[43]K. Kimura, S. Ido, N. Oyabu, K. Kobayashi, Y. Hirata, T. Imai, and H. Yamada, J. Chem. Phys. **132**, 194705 (2010).
[44]K. Hashimoto, K. Amano, N. Nishi, and T. Sakka, Chem. Phys. Lett. **754**, 137666 (2020).
[45]B. Derjaguin, Kolloid-Z. **69**, 155 (1934).
[46]K. Amano, M. Iwaki, K. Hashimoto, K. Fukami, N. Nishi, O. Takahashi, and T. Sakka, Langmuir **32**, 11063 (2016).
[47]D. A. Case, I. Y. Ben-Shalom, S. R. Brozell, D. S. Cerutti, T. E. Cheatham, V. W. D. Cruzeiro, T. A. Darden, R. E. Duke, D. Ghoreishi, M. K. Gilson, H. Gohlke, A. W. Goetz, D. Greene, R. Harris, N. Homeyer, Y. Huang, S. Izadi, A. Kovalenko, T. Kurtzman, T. S. Lee, S. LeGrand, P. Li, C. Lin, J. Liu, T. Luchko, R. Luo, D. J. Mermelstein, K. M. Merz, Y. Miao, G. Monard, C. Nguyen, H. Nguyen, I. Omelyan, A. Onufriev, F. Pan, R. Qi, D. R. Roe, A. Roitberg, C. Sagui, S. Schott-Verdugo, J. Shen, C. L. Simmerling, J. Smith, R. SalomonFerrer, J. Swails, R. C. Walker, J. Wang, H. Wei, R. M. Wolf, X. Wu, L. Xiao, D. M. York, and P. A. Kollman, AMBER2018, 2018.